Mon. Not. R. Astron. Soc. **391,** 1301–1307 (2008) doi:10.1111/j.1365-2966.2008.13956.x

The clustering and abundance of star-forming and passive galaxies at $z \sim 2$

W. G. Hartley,[1⋆] K. P. Lane,[1] O. Almaini,[1] M. Cirasuolo,[2] S. Foucaud,[1] C. Simpson,[3] S. Maddox,[1] I. Smail,[4] C. J. Conselice,[1] R. J. McLure[2] and J. S. Dunlop[5]

[1]*School of Physics and Astronomy, University of Nottingham, University Park, Nottingham NG7 2RD*
[2]*SUPA (Scottish Universities Physics Alliance), Institute for Astronomy, University of Edinburgh, Royal Observatory, Edinburgh EH9 3HJ*
[3]*Astrophysics Research Institute, Liverpool John Moores University, Twelve Quays House, Egerton Wharf, Birkenhead CH41 1LD*
[4]*Institute for Computational Cosmology, Department of Physics, Durham University, Durham DH1 3LE*
[5]*Department of Physics and Astronomy, University of British Columbia, 6224 Agricultural Rd, Vancouver, BC V6T 1Z1, Canada*

Accepted 2008 September 12. Received 2008 September 3; in original form 2008 June 10

ABSTRACT

We use the UKIRT (United Kingdom Infrared Telescope) Infrared Deep Sky Survey (UKIDSS) Ultra-deep survey (UDS), currently the deepest panoramic near-infrared survey, together with deep Subaru optical imaging to measure the clustering, number counts and luminosity function of galaxies at $z \sim 2$ selected using the *BzK* selection technique. We find that both star-forming (s*BzK*) and passive (p*BzK*) galaxies, to a magnitude limit of $K_{AB} < 23$, are strongly clustered. The passive galaxies are the most strongly clustered population, with scalelengths of $r_0 = 15.0^{+1.9}_{-2.2}\,h^{-1}$ Mpc compared with $r_0 = 6.75^{+0.34}_{-0.37}\,h^{-1}$ Mpc for star-forming galaxies. The direct implication is that passive galaxies inhabit the most massive dark matter haloes, and are thus identified as the progenitors of the most massive galaxies at the present day. In addition, the p*BzK*s exhibit a sharp flattening and potential turnover in their number counts, in agreement with other recent studies. This plateau cannot be explained by the effects of incompleteness. We conclude that only very massive galaxies are undergoing passive evolution at this early epoch, consistent with the downsizing scenario for galaxy evolution. Assuming a purely passive evolution for the p*BzK*s from their median redshift to the present day, their luminosity function suggests that only ∼2.5 per cent of present-day massive ellipticals had a p*BzK* as a main progenitor.

Key words: galaxies: evolution – galaxies: formation – galaxies: high-redshift – large-scale structure of Universe – infrared: galaxies.

1 INTRODUCTION

There is growing evidence to support the view that the most massive objects in the Universe were the first to assemble and complete their star formation (De Lucia et al. 2004; Kodama et al. 2004; Thomas et al. 2005; Bundy et al. 2006; Stott et al. 2007); this phenomenon has become known as *downsizing* (Cowie, Songaila & Barger 1999). A number of key issues remain unresolved however. There are indications that the buildup of the galaxy colour bimodality occurs around $z \sim 2$ (e.g. Cirasuolo et al. 2007), but the precise evolutionary path from the distant Universe to the present day is still undetermined. The mechanism that terminates the major episode of star formation is poorly understood (Benson, Kamionkowski & Hassani 2005), and it is now clear that massive galaxies undergo significant size evolution from $z \sim 2$ to the present day (e.g. Cimatti et al. 2008 and references therein).

Galaxy clustering is an important tool for investigating these populations, since the amplitude of clustering on large scales (>1 Mpc) can provide a measurement of the dark matter halo mass (Mo & White 1996; Sheth & Tormen 1999). In principle, therefore, one can relate galaxy populations from the distant past to the present day by tracing the evolution of dark matter haloes within the context of a framework for structure formation.

A full exploration of these issues will require large spectroscopic surveys of infrared (IR)-selected galaxies over a representative volume of the distant Universe. Such surveys are currently at an early stage, so recent work has focused on the photometric colour selection of passive versus star-forming galaxies at the crucial $z \sim 2$ epoch. The two key methods to date are the BM/BX selection (Erb et al. 2003), which is an extension of the Lyman-break dropout and the *BzK* technique (Daddi et al. 2004) which is based on *K*-band

⋆E-mail: ppxwh1@nottingham.ac.uk

© 2008 The Authors. Journal compilation © 2008 RAS

Downloaded from https://academic.oup.com/mnras/article/391/3/1301/978212 by guest on 21 August 2022

selection. Recent studies have shown that the BM/BX technique is reasonably efficient at selecting actively star-forming galaxies at $z \sim 2$, but largely misses the passive galaxy population at these epochs (Grazian et al. 2007; Quadri et al. 2007). In contrast, the *BzK* method appears to be the most complete of the broad-band techniques for the selection of both star-forming and passive galaxies (Daddi et al. 2004; van Dokkum et al. 2006; Grazian et al. 2007). Based on the initial *K*-band selection, in principle, it does not suffer the same heavy biases caused by dust or the age of the stellar populations.

An alternative is to use a larger set of filters over a range of wavelengths and infer a galaxy's redshift from comparison of the calculated magnitudes with a set of templates (Cirasuolo et al. 2007, and references therein). This work makes use of such photometric redshifts and, in principle, one can derive the stellar age of a galaxy using such templates. However, due to the uncertainties in determining stellar ages from the template fits, and the desire for comparison with the literature, the bulk of the present analysis is based on simple *BzK* selection.

The *BzK* technique was first developed using the K20 survey (Cimatti et al. 2002) by Daddi et al. (2004), and preferentially selects star-forming and passive galaxies in the redshift range $1.4 < z < 2.5$ by using the *B*-, *z*- and K_s-band broad-band filters. Recent work has shown that the number counts of these populations differ markedly (Kong et al. 2006, hereafter K06; Lane et al. 2007, hereafter L07), with star-forming galaxies being far more abundant at all magnitudes. The abundance of s*BzK* galaxies allowed K06 to perform a detailed clustering analysis, segregated by limiting *K*-band luminosity in the range $18.5 < K_{\rm vega} < 20$. They found that the clustering of s*BzK*s is strongly dependent on *K*-band luminosity. Hayashi et al. (2007) studied the clustering of s*BzK*s over a smaller area (180 arcmin^2) but to a much greater depth ($K_{AB} < 23.2$) and confirmed this strong luminosity dependence. The s*BzK* population therefore appear to inhabit a range of halo masses, and are therefore likely to be the progenitors of a wide range of present-day galaxies.

There have been fewer studies of *passive* galaxy clustering at high redshift, in part because of their relatively low surface density. K06 found early evidence that p*BzK*s are more strongly clustered than s*BzK*s, although the limited depth and area of this survey (320 arcmin^2 to $K_{\rm vega} = 20$) give rise to significant statistical uncertainly, particularly given the relatively low surface density of p*BzK*s at these magnitudes (0.38 arcmin^{-2}). Blanc et al. (2008) measured the clustering and number counts of *BzK*-selected galaxies to the same depth as K06, but over a much wider area (0.71 deg^2 total between two fields). Their *BzK* clustering amplitudes are smaller than those of K06 but consistent at the 1σ level. The analysis of deeper survey data over a similar area is required to confirm these results, and we present such an analysis in this work.

L07 used the early data release (EDR) from the UKIDSS Ultra-Deep Survey (UDS) to investigate the number counts and overlap in colour-selected galaxies, including those selected by the *BzK* technique. They found that the flattening in p*BzK* number counts observed by K06 extends to become a plateau at the EDR depth of $K_{AB} < 22.5$ and noted that if this were to continue to turnover it could imply an absence of high-redshift passive galaxies at low luminosities.

In this work, we investigate the number counts and clustering of *BzK*-selected galaxies over a substantially greater depth and area than any previous study. Section 2 describes the data and galaxy number counts. In Section 3, we present an angular clustering analysis, which is extended by deprojection to infer the real-space correlation lengths. In Section 4, we use photometric redshifts to derive a luminosity function for these populations, and compare with the present-day galaxy luminosity function. A discussion and conclusions are presented in Section 5. Throughout this paper, we assume a flat Λ cold dark matter (ΛCDM) cosmology with $\Omega_{\rm m} = 0.3$ and $h = 0.73$.

2 SOURCE IDENTIFICATION AND NUMBER COUNTS

2.1 Data set and sample definitions

The UKIRT (United Kingdom Infrared Telescope) Infrared Deep Sky Survey (UKIDSS) has been underway since spring 2005 and comprises five subsurveys covering a range of areas and depths (Lawrence et al. 2007). This survey has been made possible by the advent of the UKIRT Wide-Field Camera (Casali et al. 2007).

We base the present study on the data from the deepest component of UKIDSS, the UDS (Almaini et al., in preparation). This aims to reach final depths of $K_{AB} = 25.0$, $H_{AB} = 25.4$ and $J_{AB} = 26.0$ (5σ, point source, 2 arcsec) over an area of 0.8 deg^2. The size of the UDS field significantly reduces the effects of cosmic variance and on this scale is the deepest near-infrared survey to date. For this work we use the UDS DR1 release (Warren et al. 2007), which reaches 5σ (point source) depths of $K_{AB} = 23.5$ and $J_{AB} = 23.7$. For details of the completeness estimation, image stacking, mosaicing and catalogue extraction procedures, see Foucaud et al. (2007) and Almaini et al. (in preparation). In addition to these data, deep *B*, *V*, *R*, i', z' imaging is also available from Subaru Suprimecam to limiting depths of $B_{AB} = 28.4$, $V_{AB} = 27.8$, $R_{AB} = 27.7$, $i'_{AB} = 27.7$ and $z'_{AB} = 26.7$ (Furusawa et al. 2008). The UDS and Subaru survey areas are not entirely coincident, which reduces our usable area to 0.63 deg^2 in this analysis.

2.2 Construction of the *BzK* colour–colour diagram

The original *BzK* selection technique was introduced in Daddi et al. (2004) based on photometry in the Bessel *B* band, Gunn *z* band and K_s bands as defined on the FORS1, FORS2 and ISAAC instruments at the Very Large Telescope (VLT). To correct our colours to these filters, we used the stellar track of K06, who in turn used published empirical stellar spectra from Pickles (1998) and synthetic stellar spectra from Lejeune, Cuisinier & Buser (1997), convolved with the filter responses of the VLT instruments used in Daddi et al. (2004). These derived colours provide a convenient reference for matching stars on the well-defined *BzK* stellar locus. We use the adjusted stellar locus of K06 in the following way.

The stellar locus can be split into a main branch and a 'knee' feature, clearly visible in the lower part of Fig. 1. The intersection of these branches provides a fixed point in the *BzK* plane from which we can derive a quantitative adjustment. Using a least squares fit to each section, we derived the following offset in $z - K$ and $B - z$ colours to this fixed point to convert to the photometric system of Daddi et al. (2004):

$$(z - K)_{\rm Daddi} = (z' - K)_{\rm UDS} - 0.26, \quad (1)$$

$$(B - z)_{\rm Daddi} = (B - z')_{\rm UDS} + 0.06. \quad (2)$$

This correction is then applied to all sources in the *BzK* plane. We henceforth refer to *BzK* photometry defined in this way.

The standard *BzK* definitions of Daddi et al. (2004) were then used to construct our *BzK* sample. *K*-band sources ($>5\sigma$) from the UDS were used as the primary catalogue, with optical magnitudes

Downloaded from https://academic.oup.com/mnras/article/391/3/1301/978212 by guest on 21 August 2022

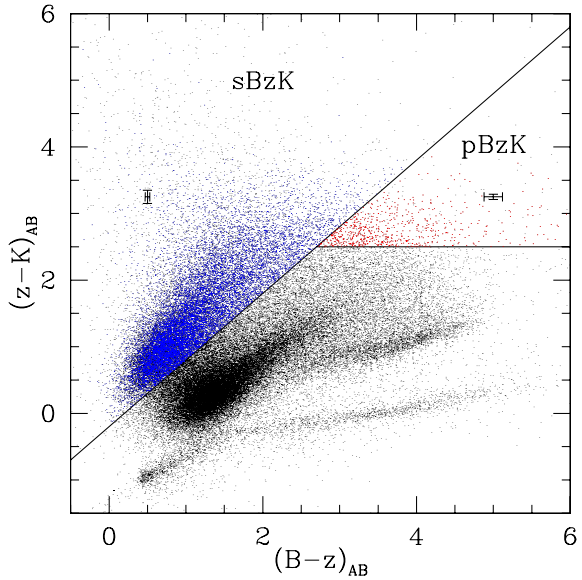

Figure 1. *BzK* colour–colour diagram for sources in the UDS DR1. The s*BzK* and p*BzK* selection regions are marked accordingly. Also visible are the passive galaxy track identified in L07, and the stellar locus used to match our photometric system to that of Daddi et al. (2004) (see the text). We show mean error bars for the galaxies in the *BzK* selection regions.

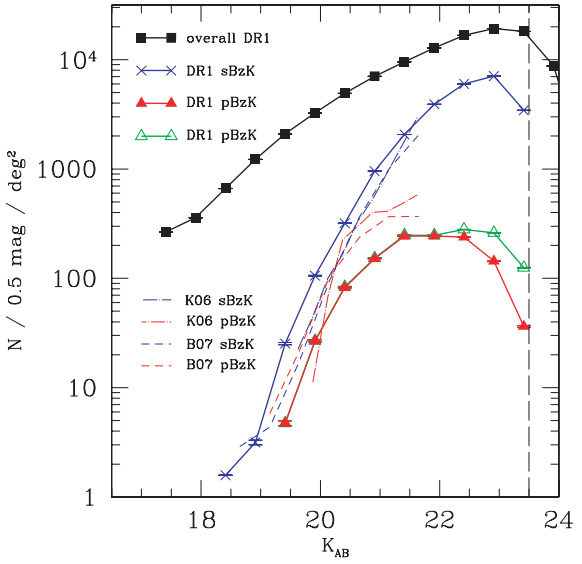

Figure 2. Differential number counts of passive and star-forming *BzK* galaxies with apparent *K*-band magnitude, compared with the full sample of *K*-selected galaxies. The error bars shown are standard Poisson errors on the counts. Two sets of values are shown for p*BzK*s: the standard selection of p*BzK*s (filled, red triangles) and the worst-case sample described in the text (open, green triangles). Numerical values are reproduced in Table 1. Literature values from K06 and Blanc et al. (2008) are also shown (dot–dashed lines and dashed lines, respectively). The plateau identified in previous works (K06; L07; Blanc et al. 2008) and subsequent turnover prior to our magnitude limit are apparent in the p*BzK* number counts.

extracted directly from the Subaru imaging data after careful matching of the Subaru and UDS astrometric frames. Aperture magnitudes were then extracted using a 2-arcsec diameter. Only sources outside the contaminated haloes of saturated optical stars were used.

All *K*-band sources with $K_{AB} < 23.5$ were used for *BzK* selection unless both the *B*- and z'-band magnitudes were fainter than the 3σ limits measured on those images (0.29 per cent of sources outside of contaminated regions), since these cannot be constrained within the *BzK* plane.

Overall, this procedure results in the selection of 15 177 s*BzK*s (21.7 per cent of the full sample) and 742 p*BzK*s (1.06 per cent of the sample), 11 551 and 702, respectively, at $K_{AB} < 23.0$.

2.3 Number counts

The differential *K*-band number counts are illustrated in Fig. 2, and tabulated in Table 1, for both the full sample of galaxies and those selected as passive and star-forming *BzK*s. We find a steep rise in the counts of star-forming s*BzK*s towards fainter magnitudes. In contrast, p*BzK* number counts exhibit an apparent flattening at $K \sim 21$, consistent with the findings of K06 and L07. Since these galaxies are sampled over a relatively narrow redshift range, this may imply that the passive population consists largely of luminous galaxies at this early epoch (see Section 4).

To investigate the reality of the turnover, we note that the galaxies around and beyond this feature have very faint *B*-band magnitudes, with a substantial fraction (62 per cent) below the 3σ detection limit in this band ($B_{\rm lim} = 28.4$). A non-detection in the *B* band does not affect their classification, however, and merely pushes them redward in $B - z$ colour in the *BzK* diagram illustrated in Fig. 1. The more worrying class are the objects which are below the 3σ limit in z' *and* *B*, which cannot be assigned *BzK* classification (164 objects). Fig. 3 shows that even within our *K*-band limit, we become incomplete above $(z - K) \simeq 3$. We study the effect of this incompleteness by considering the extreme case in which all of the objects with *B*- and z'-band magnitudes fainter than the 3σ limits (28.4 and 26.7, respectively) are p*BzK*s. In this 'worst-case' sample, the number counts still exhibit a plateau, as before, but with the absence of a turnover.

Table 1. Differential number counts in log(N/deg^2/0.5 mag) bins for s*BzK* and p*BzK* in the UDS DR1.

K-bin centre	All sources	s*BzK*	p*BzK*	Worst case p*BzK*
17.41	2.832	0.198	–	–
17.91	2.803	0.676	–	–
18.41	2.957	0.198	–	–
18.91	3.203	0.500	–	–
19.41	3.380	1.403	0.676	0.676
19.91	3.556	2.025	1.429	1.429
20.41	3.720	2.504	1.914	1.923
20.91	3.872	2.982	2.181	2.185
21.41	3.998	3.315	2.386	2.394
21.91	4.121	3.592	2.386	2.394
22.41	4.229	3.778	2.377	2.431
22.91	4.285	3.849	2.158	2.394
23.41	4.258	3.536	1.560	2.158
23.91	3.942	0.801	–	–

At our conservative limit of $K_{AB} < 23$, our completeness is >95 per cent for compact galaxies (Almaini et al., in preparation), so the feature is unlikely to be due to *K*-band incompleteness unless there is unprecedented size evolution in the p*BzK* population towards fainter magnitudes compared to the general population. The extreme compactness of passive galaxies at these redshifts observed by Cimatti et al. (2008) suggests that of the two classes, the s*BzK*s

Downloaded from https://academic.oup.com/mnras/article/391/3/1301/978212 by guest on 21 August 2022

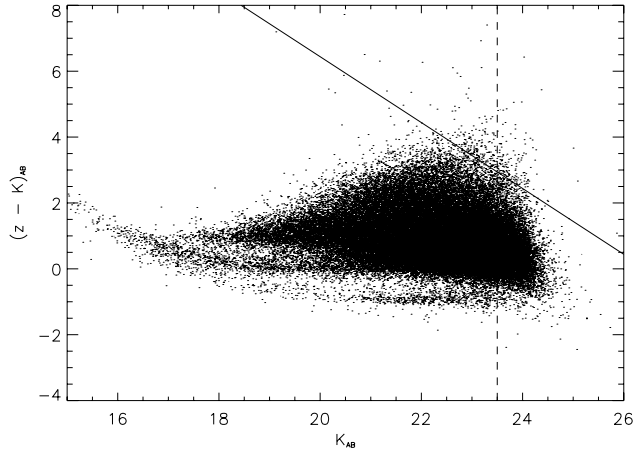

Figure 3. $(z - K)_{AB}$ colour versus *K*-band magnitude. The dashed line is our completeness limit of $K_{AB} = 23.5$ for the full sample, while the solid line shows how the completeness limit in *z* affects $(z - K)$ colour. We begin to be incomplete above $(z - K) > 2.94$. The impact of this incompleteness is discussed in the text.

should suffer more from such incompleteness. There is no evidence from their number counts to suggest that they are adversely affected in this way, so we expect that the p*BzK*s are likewise unaffected below this magnitude.

Photometric errors are another source of concern. Adjusting the boundaries for p*BzK* selection by the mean photometric errors for the sources close to the boundaries (0.1 mag), we found that such errors had no notable impact on the decline in the p*BzK* population. Additionally, since the p*BzK* region of the colour–colour plane is sparsely populated, photometric errors are likely to scatter fainter objects *into* p*BzK* selection, rather than the opposite. The faint p*BzK* counts are thus likely to be slightly *overestimated* because of photometric errors.

We conclude that the flattening in the p*BzK* population is likely to be real and the subsequent turnover is probable but not certain. We note that the turnover corresponds to absolute magnitude $M_K = -23.6$ at $z = 1.4$, which is close to the value of L^* determined for the *K*-band luminosity function at these redshifts (Cirasuolo et al. 2007). Taken at face value, these results are suggestive of a sharp decline in the number density of p*BzK* galaxies towards lower luminosities, consistent with expectation from downsizing. As correctly pointed out in Grazian et al. (2007) and predicted by Daddi et al. (2004), this is not necessarily equivalent to a true decline in the number density of passive galaxies, since the efficiency and completeness of the p*BzK* technique are largely untested at such faint magnitudes. In particular, there is some evidence that passive galaxies can also be found among the redder s*BzK* galaxies (at large values of $z - K$), with a possible incompleteness as high as 34 per cent (Grazian et al. 2007). We find that randomly adding an additional 34 per cent of galaxies to the p*BzK* sample from this part of the diagram is indeed sufficient to remove the apparent turnover, since these are predominantly the fainter s*BzK* galaxies.

The s*BzK* number counts are significantly higher than those of K06, Blanc et al. (2008) and Imai et al. (2008) (not plotted); while the p*BzK* number counts are lower. The UDS field is more than six times larger than that of the K20 survey and four times larger than the one used in Imai et al. (2008). The combined field used in Blanc et al. (2008) is of a similar size to the UDS; cosmic variance is the most likely explanation for the difference in number counts in this case.

3 CLUSTERING PROPERTIES

3.1 Angular clustering

The two-point angular correlation function, $w(\theta)$, is defined by the joint probability of finding two galaxies in solid-angle elements $\delta\Omega_1$ and $\delta\Omega_2$ at a given separation (Peebles 1980):

$$\delta P = n^2 \delta\Omega_1 \delta\Omega_2 [1 + w(\theta_{12})]. \quad (3)$$

To estimate the correlation function, we use the estimator of Landy & Szalay (1993):

$$w(\theta) = \frac{DD - 2DR + RR}{RR}, \quad (4)$$

where *DD*, *DR* and *RR* are the counts of data–data, data–random and random–random pairs, respectively, at an angular separation θ, normalized by the total number possible. Although this estimator is relatively robust against systematic errors, there remains a small bias due to the finite field size, which is corrected for an integral constraint by a constant, C. We follow the method of Roche & Eales (1999) by using the random–random counts to estimate the size of this bias:

$$C = \frac{\Sigma N_{\rm RR}(\theta)\theta^{-0.8}}{\Sigma N_{\rm RR}(\theta)}, \quad (5)$$

where the sums extend to the largest separations within the field.

The s*BzK* and p*BzK* samples were selected to a limit of $K_{AB} < 23$. We adopted this conservative magnitude limit to ensure the minimum contamination by spurious sources. We fit a single power law of the form $w(\theta) = A(\theta^{-\delta} - C)$ to the corrected data over the separation range 0.01°–0.1°, fixing the slope to the fiducial $\delta = 0.8$ and minimizing the χ^2. The errors on the measurements are a combination of those due to shot noise (estimated by bootstrap resampling) and an estimate of those due to cosmic variance. The estimates for cosmic variance were found by splitting the field into four and computing the variance of $w(\theta)$.

In order to fit the clustering reliably, we wish to avoid small-scale excesses due to multiple-galaxy occupation of a single halo. The lower bound was chosen to correspond to ∼0.9 Mpc (comoving) at $z \sim 2$ for this reason. The upper bound is a conservative estimate of the limit to which our data have enough signal for a reliable fit to be obtained.

For s*BzK* galaxies, the amplitude was found to be $A = 1.79^{+0.17}_{-0.17} \times 10^{-3}$ (deg$^{0.8}$), and for the p*BzK* population $A = 6.37^{+1.58}_{-1.54} \times 10^{-3}$ (deg$^{0.8}$). The clustering amplitude of the p*BzK*s is inconsistent with the clustering of s*BzK* galaxies at the 3σ level. Fig. 4 shows the clustering measurements corrected for the integral constraint for the s*BzK* and p*BzK* galaxies.

3.2 Deprojected clustering amplitude

The real-space clustering and projected clustering are linked by the relativistic Limber equation (Limber 1954). If the redshift distribution of a sample is known, the Limber equation can be inverted and the correlation length, r_0, can be calculated in a robust manner (Peebles 1980; Magliocchetti & Maddox 1999)

To estimate the redshift distribution, we use photometric redshifts based on the Subaru and UDS bands previously introduced, with the addition of *Spitzer* data taken as part of the SIRFT Wide-Area Infrared Extragalactic Survey (SWIRE) survey (Lonsdale et al. 2003). The method is described fully in Cirasuolo et al. (2007), and consists of minimizing the χ^2 of synthetic galaxy templates. The distributions are shown in Fig. 5. The photometric redshift distribution was

Downloaded from https://academic.oup.com/mnras/article/391/3/1301/978212 by guest on 21 August 2022

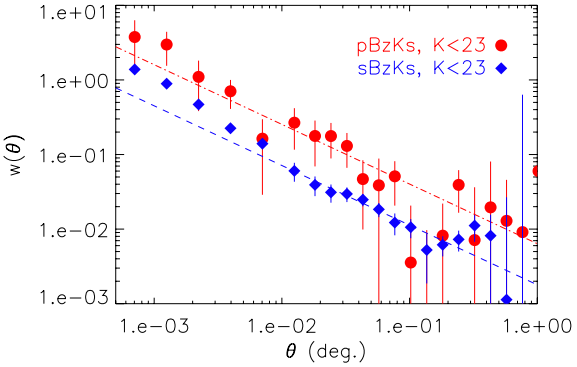

Figure 4. The angular correlation function for our *BzK*-selected galaxy samples. The best-fitting power laws are shown, with slopes fixed to the fiducial value of $\delta = 0.8$. The p*BzK* galaxies are very strongly clustered, much more than s*BzK*s, indicating that they occupy the most massive dark matter haloes at their epoch.

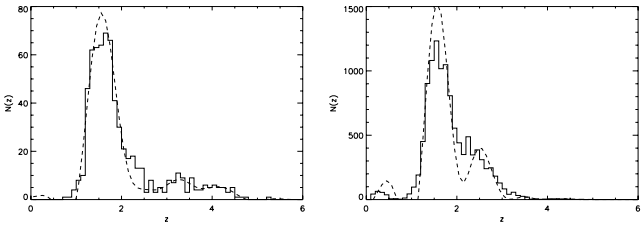

Figure 5. Photometric redshift distributions for passive (left-hand panel) and star-forming (right-hand panel) *BzK*-selected galaxies (solid line histogram). The overplotted dashed lines are distributions with photometric errors de-convolved (see the text).

then used directly in the inverted Limber's equation during the calculation of r_0. The values obtained in this manner are $r_0 = 15.8^{+2.0}_{-2.2}$ and $7.69^{+0.40}_{-0.41}\,h^{-1}$ Mpc for $K < 23$ p*BzK*s and s*BzK*s, respectively. The quoted errors are due to the error in the fit to the clustering amplitude and therefore take into account the shot noise and cosmic variance.

The photometric redshifts are subject to errors [$\sigma/(1+z) = 0.095$ and 0.105 for p*BzK*s and s*BzK*s, respectively], however, and assuming that the true redshift distribution is highly peaked, these errors are likely to broaden the measured distribution. A broader distribution will result in a larger inferred clustering scalelength. It is therefore important that we take such errors into account. We do so by assuming the errors are Gaussian, and then deconvolve the errors from the redshift distribution using a Fourier-based Wiener filter. A more detailed description of this method is provided in the appendix. The resulting deconvolved redshift distributions are shown in Fig. 5.

The scaling lengths recovered using the corrected redshift distribution are as follows: $15.0^{+1.9}_{-2.2}$ and $6.75^{+0.34}_{-0.37}\,h^{-1}$ Mpc for p*BzK*s and s*BzK*s, respectively.

However, we note that our photometric redshift code is largely untested for p*BzK* and s*BzK* galaxies. This work will be refined by the use of an ongoing European Southern Observatory (ESO) Large Programme using VIMOS and FORS2 on the VLT to target one-sixth of the UDS DR1 galaxies with photometric redshifts >1.

We also confirm previous claims for a dependence of s*BzK* clustering on apparent magnitude (Hayashi et al. 2007). Fig. 6 and Table 2 show the values for s*BzK*s with varying limiting magnitude.

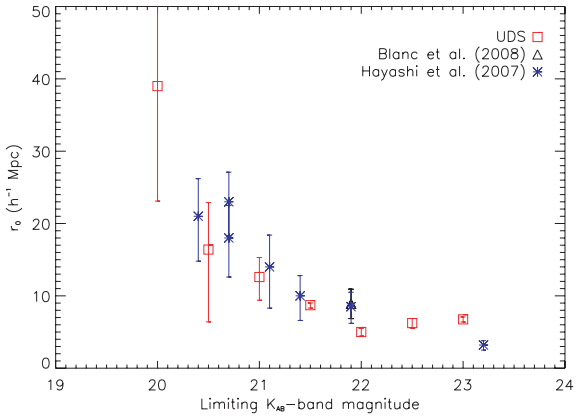

Figure 6. The dependence of clustering strength of s*BzK*-selected galaxies on limiting K_{AB}-band magnitude. Our measurements (open squares) are shown together with literature values from Blanc et al. (2008) and Hayashi et al. (2007) (open triangle and asterisks, respectively). Our values confirm the magnitude dependence of sBzK clustering strength.

Table 2. Values of r_0 for s*BzK*s in the UDS by limiting K_{AB}-band magnitude along with the number of objects brighter than the relevant limit. As for the full samples, the error ranges are derived from estimates of the shot noise and cosmic variance.

$K_{AB,\mathrm{lim}}$	N	r_0
20.0	92	$39.0^{+11.8}_{-15.9}$
20.5	250	$16.4^{+6.5}_{-10.0}$
21.0	689	$12.6^{+2.7}_{-3.2}$
21.5	1724	$8.71^{+1.49}_{-1.68}$
22.0	3789	$5.00^{+0.49}_{-0.55}$
22.5	7199	$6.23^{+0.64}_{-0.69}$
23.0	11 551	$6.75^{+0.34}_{-0.37}$

The dependence is much stronger at magnitudes of $K < 22$, indicating a strong correlation between halo mass and s*BzK* luminosity for these objects.

3.3 *BzK* galaxies selected at $1.4 < z < 2.5$

The *BzK* selection was defined by Daddi et al. (2004) to isolate galaxies in the redshift range $1.4 < z < 2.5$. Clearly from Fig. 5, and as expected by Daddi et al. (2004), there are contaminating objects from outside of this range. Using our photometric redshifts, we can access how successful the *BzK* selection technique is in reproducing the clustering of objects within the desired range.

Following the same method outlined for the full samples, we compute clustering amplitudes and find correlation lengths of $11.1^{+1.7}_{-1.8}$ and $5.46^{+0.36}_{-0.37}\,h^{-1}$ Mpc for $1.4 < z < 2.5$ p*BzK*s and s*BzK*s, respectively. These values are slightly lower than those for the full samples and indicate that the high-redshift tails in the full sample are at least as highly clustered as those within the $1.4 < z < 2.5$ range. However, the conclusions drawn from the full sample are still valid, namely that the p*BzK* galaxies are significantly more strongly clustered than the s*BzK* galaxies.

Downloaded from https://academic.oup.com/mnras/article/391/3/1301/978212 by guest on 21 August 2022

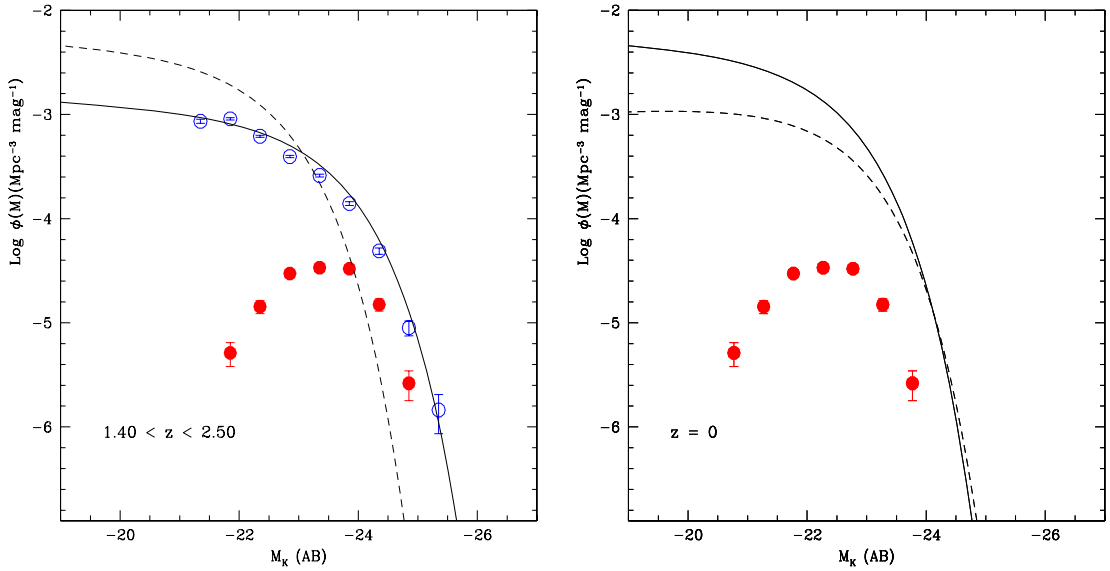

Figure 7. Left-hand panel: luminosity functions for our pBzK and s*BzK* samples (filled and open circles, respectively), plus all *K*-selected galaxies to a limit of $K < 23$ (restricted to galaxies with photometric redshifts in the range $1.4 < z < 2.5$, solid line). The s*BzK*s are representative of the overall population in the range $1.4 < z < 2.5$, while the p*BzK*s are found to be exclusively bright objects. Also shown is the $z = 0$ luminosity function for *K*-selected galaxies from Kochanek et al. (2001) (dashed line). Right-hand panel: the solid line shows the same luminosity function for $z = 0$ galaxies as the dashed line in the right-hand panel. The dashed curve shows the $z = 0$ luminosity function for early-type galaxies from Kochanek et al. (2001), while the points are the $z = 0$ luminosity function for p*BzK*s under the assumption of passive evolution (see the text).

4 LUMINOSITY FUNCTION

A luminosity function was constructed for our *BzK*-selected galaxies in the same way as detailed in Cirasuolo et al. (2007), by using the $1/V_{\rm max}$ method (Schmidt 1968). Fig. 7 shows the luminosity function for the *BzK* galaxies with photometric redshifts in the range $1.4 < z < 2.5$ (points with error bars), compared with all *K*-selected galaxies in the same range (solid line). Also plotted is the $z = 0$ luminosity function from Kochanek et al. (2001). It is clear that s*BzK* galaxies sample a wide range in luminosity, while the p*BzK* population are dominated by bright galaxies with $M_K > -23$. At this epoch, however, the bright end of the luminosity function is still dominated by star-forming objects, consistent with Cirasuolo et al. (2007) who found that the galaxy colour bimodality is weak at these redshifts. The p*BzK* galaxies are nevertheless likely to be among the most massive systems, since the mass-to-light ratio will be significantly lower for the actively star-forming systems.

Under the assumption that the p*BzK*s passively evolve to the present day (with minimal merging), one can estimate their contribution to the bright end of the present-day luminosity function. The implied evolution is modelled from $z \sim 1.60$ (the median value for p*BzK*s) to $z = 0$ assuming the spectral evolution models of Bruzual & Charlot (2003). For simplicity, we chose a solar metalicity model and a Salpeter initial mass function (Salpeter 1955) and assume only passive evolution from initial formation bursts at redshifts $z_f = 3$ and 10. This results in a Johnson *K*-band absolute magnitude evolution in the range $0.96 < \Delta M_K < 1.21$. Taking the mean value, we can estimate the minimum number of present-day bright ($K < -23.4$) galaxies that could previously have been p*BzK*s. Under our assumptions we find that 2.5 per cent of such galaxies can be explained by passively evolved p*BzK*s. It is assumed that the remainder is made up of the descendants of bright s*BzK*s and merger remnants from within and between the two classes.

5 DISCUSSION AND CONCLUSIONS

We present the number counts, clustering and luminosity function of galaxies at $z \sim 2$ selected using the *BzK* selection criteria. The p*BzK* galaxies show a marked flattening in their number counts which cannot be explained by the effects of incompleteness, and a possible turnover at faint magnitudes. We conclude that, at this epoch, it is generally luminous, massive galaxies that are undergoing passive evolution. This is consistent with the downsizing scenario, in which the most massive galaxies are formed first and are the first to evolve on to the red sequence (Kodama et al. 2004).

The angular clustering of the passive galaxy sample is very strong, approximately four times the amplitude of the s*BzK* population. This is, in part, due to their relatively narrow redshift distribution (K06), but a large difference remains after derojection to the real-space correlation length. We find $r_0 = 15.0^{+1.9}_{-2.2}$ and $6.75^{+0.34}_{-0.37}\,h^{-1}$ Mpc for the p*BzK* and s*BzK* galaxies, respectively. Our value for the correlation length of s*BzK*s is almost twice that found by Hayashi et al. (2007), who used a sample with similar limiting magnitude but with smaller field size (180 arcmin^2, compared with $\sim$2250 arcmin^2 for the UDS). Our sample consists of more than 10 times the number of s*BzK*s than that of Hayashi et al. (2007) and, in addition, we make fewer assumptions regarding their redshift distribution. Further surveys reaching depths of $K_{AB,\rm lim} \sim 23$ are required to fully account the effects of cosmic variance, however.

We also confirm that the scalelength for the clustering of s*BzK* galaxies is dependent on apparent magnitude, consistent with the work of Hayashi et al. (2007) (Fig. 6). This dependence is far more significant at magnitudes below $K_{AB} \sim 22$, indicating a strong correlation between such galaxies, and the mass of the hosting halo.

In addition to this luminosity dependence, there is a clear enhancement at small scales in the s*BzK* clustering. This enhancement is indicative of multiple s*BzK* galaxies occupying a single dark matter halo. The scale at which this turn-off occurs can provide an indication of the size, and hence mass, of the hosting dark matter

Downloaded from https://academic.oup.com/mnras/article/391/3/1301/978212 by guest on 21 August 2022

haloes. The turn-off occurs at $\sim$0.01, which corresponds to $\sim$0.3 Mpc at $z = 1.65$. Haloes of this size have masses between 10^{11} and $10^{12}\,M_\odot$ (Mo & White 2002). A full consideration of this enhancement within the halo occupation distribution framework will be presented in a future paper. The host halo mass can also be derived from comparing the deprojected clustering scalelength with models of dark matter halo clustering evolution. Using models based on Mo & White (2002), we find a typical halo mass of $\sim 6 \times 10^{11}\,M_\odot$.

Applying the model of clustering evolution to the p*BzK*s, we can qualitatively conclude that they are inhabitants of the most massive haloes at their epoch (in excess of $10^{13}\,M_\odot$); haloes which will eventually become massive groups and clusters by the present day. The evolutionary path that p*BzK*s take with redshift will also be the subject of future work, using further colour selection techniques.

Our conclusion based on the r_0 measurement is strengthened by their luminosity function. Even under the strict assumption of purely passive evolution, the descendants of p*BzK*s occupy the bright end of the luminosity function. Such galaxies are group- and cluster-dominant galaxies in the local Universe. The brightest ($K < 21$) s*BzK*s have clustering scalelengths comparable to, or greater than, that which we have found for the p*BzK*s. This finding indicates that such galaxies will also become group and cluster-dominant galaxies by $z = 0$. The implication is that we are indeed witnessing the epoch at which the buildup of the red sequence begins.

ACKNOWLEDGMENTS

OA, IRS and RJM acknowledge the support of the Royal Society. SF, MC, KPL and WGH acknowledge the support of STFC. We are grateful to Xu Kong for help in matching photometric filters and also to Kaz Sekiguchi and Hisanori Furusawa for the Subaru data used in this study. We also extend out gratitude to the staff at UKIRT for their tireless efforts to ensure that the UKIDSS are a success. We would also like to thank the anonymous referee for their thorough reading and useful comments.

REFERENCES

Benson A. J., Kamionkowski M., Hassani S. H., 2005, MNRAS, 357, 847
Blanc G. A. et al., 2008, ApJ, 681, 1099
Bruzual G., Charlot S., 2003, MNRAS, 344, 1000
Bundy K. et al., 2006, ApJ, 651, 120
Casali M. et al., 2007, A&A, 467, 777
Cimatti A. et al., 2002, A&A, 381, L68
Cimatti A. et al., 2008, A&A, 482, 21
Cirasuolo M. et al., 2007, MNRAS, 380, 585
Cowie L. L., Songaila A., Barger A. J., 1999, AJ, 118, 603
Daddi E., Cimatti A., Renzini A., Fontana A., Mignoli M., Pozzetti L., Tozzi P., Zamorani G., 2004, ApJ, 617, 746
De Lucia G. et al., 2004, ApJ, 610, L77
Erb D. K., Shapley A. E., Steidel C. C., Pettini M., Adelberger K. L., Hunt M. P., Moorwood A. F. M., Cuby J.-G., 2003, ApJ, 591, 101
Foucaud S. et al., 2007, MNRAS, 376, L20
Furusawa H. et al., 2008, ApJS, 176, 1
Grazian A. et al., 2007, A&A, 465, 393
Hagashi M., Shimasaku K., Motohara K., Yoshida M., Okamura S., Kashikawa N., 2007, ApJ, 660, 72
Imai K., Pearson C. P., Matsuhara H., Wada T., Oyabu S., Takagi T., Fujishiro N., Hanami H., 2008, ApJ, 683, 45
Kochanek C. S. et al., 2001, ApJ, 560, 566
Kodama T. et al., 2004, MNRAS, 350, 1005
Kong X. et al., 2006, ApJ, 638, 72 (K06)
Landy S. D., Szalay A. S., 1993, ApJ, 412, 64
Lane K. P. et al., 2007, MNRAS, 379, L25 (L07)
Lawrence A. et al., 2007, MNRAS, 379, 1599
Lejeune T., Cuisinier F., Buser R., 1997, A&AS, 125, 229
Limber D. N., 1954, ApJ, 119, 655
Lonsdale C. J. et al., 2003, PASP, 115, 897
Magliocchetti M., Maddox S. J., 1999, MNRAS, 306, 988
Mo H. J., White S. D. M., 1996, MNRAS, 282, 347
Mo H. J., White S. D. M., 2002, MNRAS, 336, 112
Peebles P. J. E., 1980, The Large-Scale Structure of the Universe. Princeton University Press, Princeton, NJ
Pickles A. J., 1998, PASP, 110, 863
Quadri R. et al., 2007, AJ, 134, 1103
Roche N., Eales S. A., 1999, MNRAS, 307, 703
Salpeter E. E., 1955, ApJ, 121, 161
Schmidt M., 1968, ApJ, 151, 393
Sheth R. K., Tormen G., 1999, MNRAS, 308, 119
Stott J. P., Smail I., Edge A. C., Ebeling H., Smith G. P., Kneib J.-P., Pimbblet K. A., 2007, ApJ, 661, 95
Thomas D., Maraston C., Bender R., Mendes de Oliveira C., 2005, ApJ, 621, 673
van Dokkum P. G. et al., 2006, ApJ, 638, L59
Warren S. J. et al., 2007, MNRAS, 375, 213

APPENDIX A

In this appendix, we describe the Fourier method used to deconvolve photometric redshift errors from the $n(z)$ distribution, which can then be used to invert the Limber equation. The errors in the photometric redshift distribution are assumed to be Gaussian and it is also assumed that the measured distribution is simply the convolution of these errors with the true redshift distribution. Under these assumptions, it should be possible to deconvolve the errors from the measured distribution, using the fact that a convolution is simply a multiplication in the Fourier domain. Dividing the Fourier transform of the measured distribution by that of the Gaussian errors should then give us an estimate of the true distribution.

In practice, a relatively large number of terms in the discreet Fourier transform are required to reproduce the redshift distribution accurately, and as the Fourier transform of a Gaussian is also a Gaussian, small levels of high-frequency noise can be amplified greatly to give a spurious result. One way to avoid such a problem is to use a Wiener filter:

$$W(k) = \frac{1}{H(k)} \times \left[\frac{H(k)^2}{H(k)^2 + \frac{1}{\mathrm{SNR}}} \right], \tag{A1}$$

where $H(k)$ is the Fourier transform of the Gaussian errors and SNR is the signal-to-noise ratio. In the limit of SNR being infinite, this filter tends to $1/H(k)$ as in the simple deconvolution above. SNR is estimated by fitting the power spectrum of the redshift distribution to a function of the form $a10^{-bk} + c$, with c identified as being the noise level. The resultant redshift distributions are shown in Fig. 5.

This paper has been typeset from a TEX/LATEX file prepared by the author.

Downloaded from https://academic.oup.com/mnras/article/391/3/1301/978212 by guest on 21 August 2022